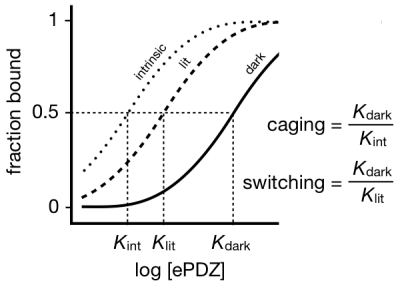

Supplementary Figure 1 Definition of caging and switching. The schematic plot depicts the fraction of LOVpep bound vs. ePDZ concentration for a photoswitchable interaction. Caging is the dark-state diminishment of binding affinity relative to the intrinsic binding affinity. Switching is the dark-state diminishment of binding affinity relative to the lit-state binding affinity.

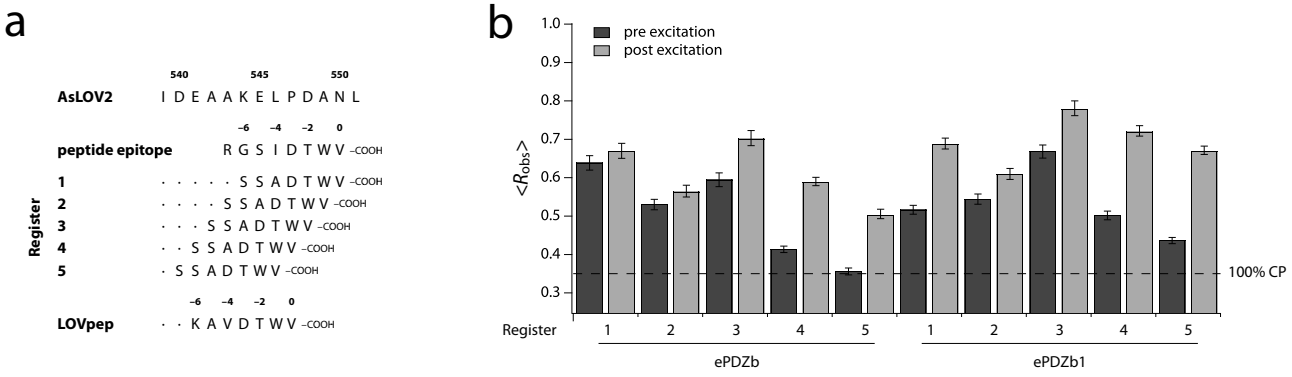

Supplementary Figure 2 Register series of LOV–peptide fusions. (**a**) Partial sequences of AsLOV2, a high-affinity ePDZ epitope, and LOV–peptide fusion constructs in 5 different registers used in **b**. AsLOV2 positions are numbered as in phototropin 1. Dots in fusion constructs denote identity with the AsLOV2 sequence. (**b**) Lit- and dark-state $<R_{obs}>$ for fusions in registers 1–5. Data are the means from a population ($n \geq 37$) of cells. Error bars, s.e.m. The dashed horizontal line represents the estimated $<R_{obs}>$ for ~100% cytoplasmic ePDZ–mCherry.

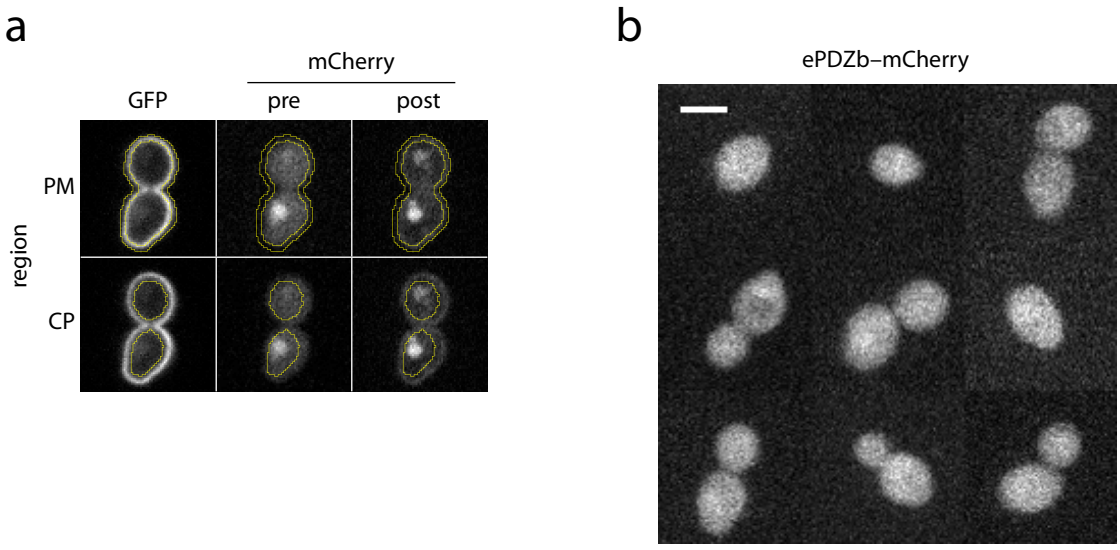

Supplementary Figure 3 Thresholding of cells for the PM recruitment assay. (**a**) Representative examples of plasma membrane (PM) and cytoplasm (CP) thresholded regions. $\langle R_{obs} \rangle$ is the ratio of PM:CP mCherry fluorescence, averaged over a population of cells. (**b**) A montage of representative cells with $R_{obs} \approx 0.35$. Scale bar, 5 μm.

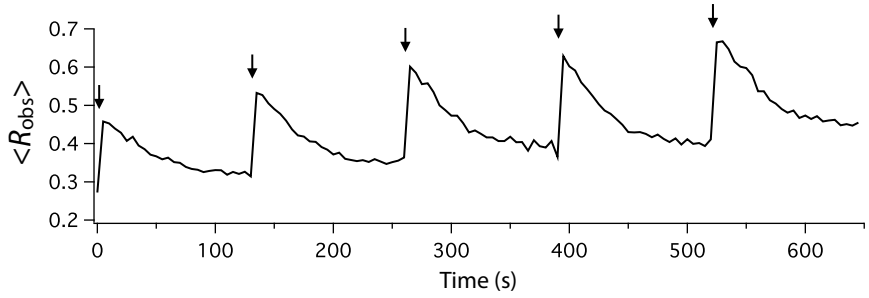

Supplementary Figure 4 Reversible light-triggered recruitment of ePDZb by LOVpep. A population of cells ($n = 6$) was repeatedly photoexcited for 1.125 second (arrows), and allowed to recover.

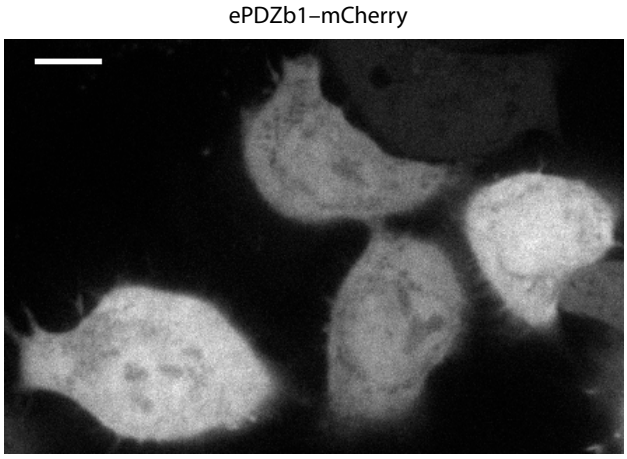

Supplementary Figure 5 ePDZ–mCherry localization in HeLa cells in the absence of LOVpep. Scale bar, 10 μm.

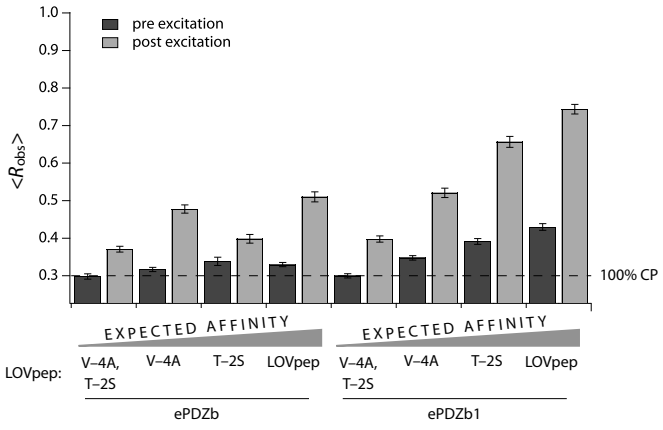

Supplementary Figure 6 Lit- and dark-state $<R_{obs}>$ using LOVpep mutations in the peptide epitope. Data are the means from a population ($n \geq 31$) of cells; error bars, s.e.m. The dashed line represents $<R_{obs}>$ for ~100% cytoplasmic ePDZ–mCherry.

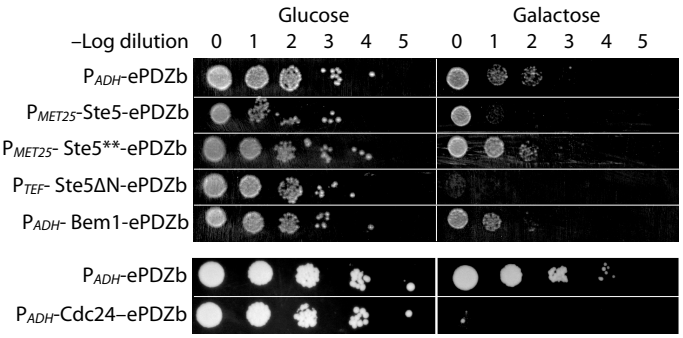

Supplementary Figure 7 Growth arrest assay for ePDZ fusions. Serial dilutions of cells were spotted onto solid media. Expression of Mid2–GFP–LOVpep^{CA} was induced or repressed with 2% galactose or 2% glucose, respectively.

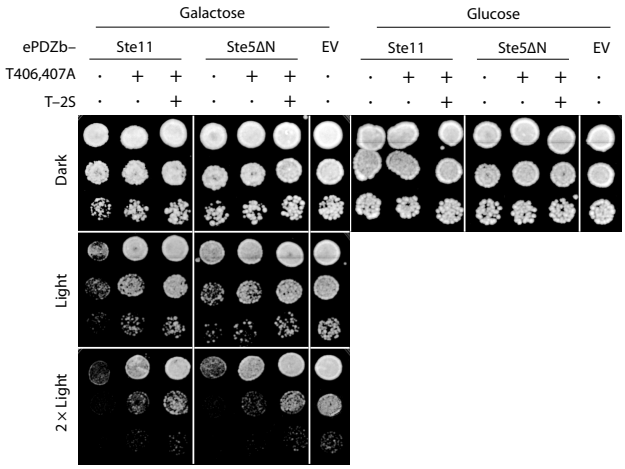

Supplementary Figure 8 Light induced growth arrest by MAPK activation. (**a**) Growth arrest by recruitment of Ste11–ePDZ and ePDZb–Ste5ΔN to Mid2(SS/TM)–GFP–LOVpep. LOVpep constructs have the T406A, T407A, and T–2S mutations as indicated. All LOVpep constructs are slow cycling (V416I). 3 dilutions (10-fold) are shown for each condition, arranged vertically.

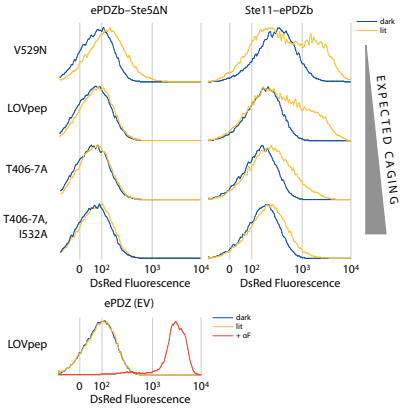

Supplementary Figure 9 P_{FUS1}–DsRed reporter activation for ePDZb–Ste5ΔN and Ste11–ePDZb constructs measured using flow cytometry. Mid2(SS/TM)–GFP–LOVpep constructs have the T406A, T407A, V529N and I532A mutations as indicated. All LOVpep constructs are slow cycling (V416I).

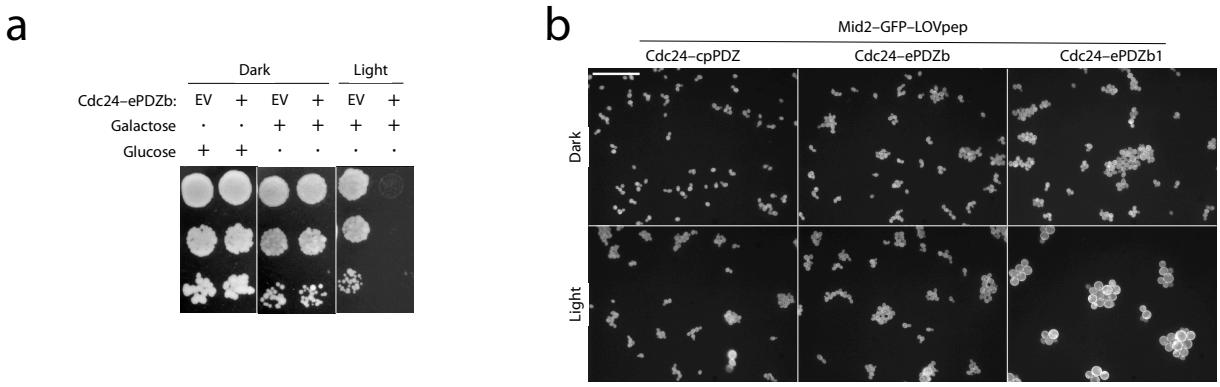

Supplementary Figure 10 Light induced growth arrest by polarity disruption. (**a**) Growth arrest on solid media by recruitment of Cdc24–ePDZb to Mid2–GFP–LOVpep. 3 dilutions (10-fold) are shown for each condition, arranged vertically. (**b**) Terminal phenotype in liquid culture caused by light-dependent global recruitment of the Cdc42 GEF Cdc24. Cdc24 is fused to PDZ, ePDZb, or ePDZb1 as indicated and globally recruited to PM-tethered LOVpep. Scale bar, 50 µm.

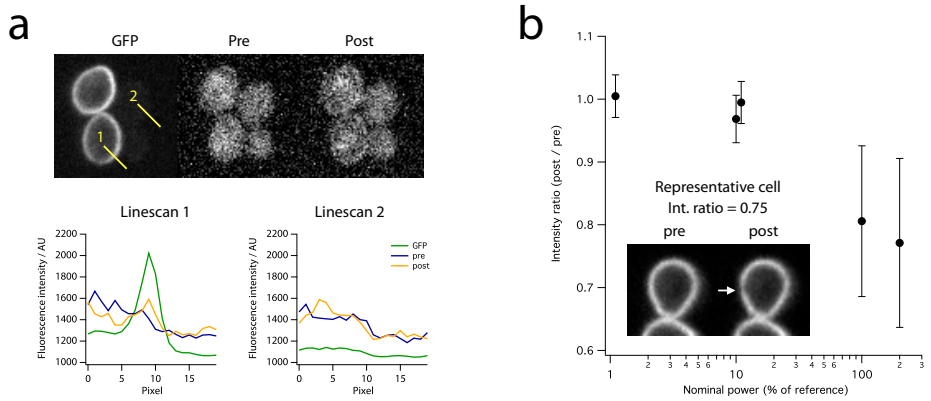

Supplementary Figure 11 Photoexcitation requirements. (**a**) Global recruitment using minimal global illumination. Cells were illuminated with a 0.063 s pulse of 0.038 J·cm^{-2}. The plots show pixel intensities measured along the yellow lines in the image. (**b**) GFP bleaching vs. Micropoint laser power. The *y*-axis is the fraction of GFP fluorescence remaining after spot illumination. The *x*-axis is the laser power. 100% nominal power is the minimal power required to ablate a thin-metal-coated slide when calibrating Micropoint steerable laser. GFP bleaching (white arrow) is nearly undetectable at 10% of this power. Spot photoexcitation experiments were conducted using 1% of the reference power.

Supplementary Table 1 Fitted values of k_{obs} and k_{phot}

		in vivo			
		LOVpep		**LOVpep V416I**	
	Imid. (mM)	**k_{obs} (s^{-1})**	**Fold-chg.**	**k_{obs} (s^{-1})**	**Fold-chg.**
ePDZb1	0	0.028	—	0.0025	—
	10	0.061	2	0.013	5
	20	0.17	6	0.044	18
ePDZb	0	0.041	—	0.0023	—
	10	0.078	2	0.011	5
	20	0.27	7	0.074	32

		in vitro			
		LOVpep		**LOVpep V416I**	
	Imid. (mM)	**k_{phot} (s^{-1})**	**Fold-chg.**	**k_{phot} (s^{-1})**	**Fold-chg.**
	0	0.036	—	0.0027	—
	10	0.15	4	0.065	24
	20	0.24	6	0.12	44

Supplementary Table 2 Fitted parameters for dissociation from spot recruitment

	LOVpep				LOVpep V416I			
	a_1	k_1 (s^{-1})	a_2	k_2 (s^{-1})	a_1	k_1 (s^{-1})	a_2	k_2 (s^{-1})
Spot + global, 2 exp.	1.03	0.027	0.25	0.18	0.25	0.0023	0.6	0.055
Spot + global, 1 exp.	—	0.035	—	—	—	ND	—	—
Spot only, 1 exp.	—	0.022	—	—	—	0.0037	—	—

ND, not determined.

Supplementary Table 3 Yeast plasmids used in this study

AsLOV2–peptide plasmids

Plasmid	Addgene ID	Type	Prom.	CDS	Details	Marker
pDS145		CEN	TEF	Pma1–GFP–LOVpep	LOVpep K–6R,T–2S	HIS3
pDS145–Hof1		CEN	TEF	Hof1–GFP–LOVpep	LOVpep K–6R,T–2S	HIS3
pDS145–Pil1		CEN	TEF	Pil1–GFP–LOVpep	LOVpep K–6R,T–2S	HIS3
pDS240	34966	YIplac	GAL1	Mid2(SS/TM)–GFP–LOVpep^{CA}	K533Δ, high-affinity epitope	LEU2
pDS247	34967	YIPlac	GAL1	Mid2(SS/TM)–GFP–LOVpep	LOVpep T406A,T407A,V416I,T–2S	LEU2
pDS248	34968	YIPlac	GAL1	Mid2(SS/TM)–GFP–LOVpep	LOVpep T406A,T407A,V416I	LEU2
pDS250	34969	YIPlac	GAL1	Mid2(SS/TM)–GFP–LOVpep	LOVpep V416I	LEU2
pDS255	34970	YIPlac	GAL1	Mid2(SS/TM)–GFP–LOVpep	LOVpep T406A,T407A	LEU2
pDS257	34971	YIPlac	GAL1	Mid2(SS/TM)–GFP–LOVpep		LEU2
pDS264		CEN	TEF	Mid2–GFP–AsLOV2–peptide	AsLOV2–(404–543)–SSADTWV	LEU2
pDS265		CEN	TEF	Mid2–GFP–AsLOV2–peptide	AsLOV2–(404–542)–SSADTWV	LEU2
pDS266		CEN	TEF	Mid2–GFP–AsLOV2–peptide	AsLOV2–(404–541)–SSADTWV	LEU2
pDS267		CEN	TEF	Mid2–GFP–AsLOV2–peptide	AsLOV2–(404–540)–SSADTWV	LEU2
pDS268		CEN	TEF	Mid2–GFP–AsLOV2–peptide	AsLOV2–(404–539)–SSADTWV	LEU2
pDS271	34974	CEN	TEF	Mid2–GFP–LOVpep	LOVpep T406A,T407A,V416I	LEU2
pDS272	34975	CEN	TEF	Mid2–GFP–LOVpep	LOVpep T406A,T407A	LEU2
pDS275	34972	YIplac	GAL1	Mid2(SS/TM)–GFP–LOVpep	LOVpep T406A,T407A,I532A	LEU2
pDS277	34973	YIplac	GAL1	Mid2(SS/TM)–GFP–LOVpep	LOVpep V529N	LEU2
pDS287		CEN	TEF	Mid2–GFP–LOVpep	LOVpep T406A,T407A	LEU2
pDS288		CEN	TEF	Mid2–GFP–LOVpep		LEU2
pDS289		CEN	TEF	Mid2–GFP–LOVpep	LOVpep T406A,T407A,I532A	LEU2
pDS290		CEN	TEF	Mid2–GFP–LOVpep	LOVpep V529N	LEU2
pDS291		CEN	TEF	Mid2–GFP–LOVpep	LOVpep I532A,T–2S	LEU2
pDS292		CEN	TEF	Mid2–GFP–LOVpep	LOVpep I532A,V–4A,T–2S	LEU2
pDS293		CEN	TEF	Mid2–GFP–LOVpep	LOVpep I532A	LEU2
pDS294		CEN	TEF	Mid2–GFP–LOVpep	LOVpep I532A,V–4A	LEU2

ePDZ plasmids

Plasmid		Type	Prom.	CDS	Details	Marker
pDS111		CEN	MET25	ePDZb–mCherry		URA3
pDS177		CEN	ADH	BEM1–ePDZb–mCherry		URA3
pDS190	34977	CEN	ADH	ePDZb		URA3
pDS191	34978	CEN	TEF	ePDZb		URA3
pDS196		CEN	MET25	Ste5–ePDZb		URA3
pDS197		CEN	MET25	Ste5**–ePDZb	Ste5 V763A,S861P	URA3
pDS206		CEN	TEF	ePDZb–Ste5ΔN (275–917)		URA3
pDS220	34980	YIplac	TEF	ePDZb–mCherry		URA3
pDS221	34981	YIplac	TEF	ePDZb1–mCherry		URA3
pDS244	34982	CEN	ADH	ePDZb–Ste11		URA3
pDS282	34983	YIplac	TEF	cpPDZ–mCherry		URA3
pDS299		YIplac	GAL1	Cdc24–ePDZb		URA3
pDS300		YIplac	GAL1	Cdc24–ePDZb1		URA3
pDS301		YIplac	GAL1	Cdc24–PDZ		URA3
pELW1040		CEN	ADH	Cdc24–ePDZb		URA3

Supplementary Table 4 Strains used in this study

Bkgd	Name	Plasmid 1	Plasmid 2	Figure(s)
a	YLS2365	pDS264	pDS220	1d
a	YLS2366	pDS265	pDS220	1d
a	YLS2367	pDS266	pDS220	1d
a	YLS2368	pDS267	pDS220	1d
a	YLS2369	pDS268	pDS220	1d
a	YLS2370	pDS264	pDS221	1d
a	YLS2371	pDS265	pDS221	1d
a	YLS2372	pDS266	pDS221	1d
a	YLS2373	pDS267	pDS221	1d
a	YLS2374	pDS268	pDS221	1d
b	—	pDS145	pDS111	2b
b	—	pDS145–Hof1	pDS111	2b
b	—	pDS145–Pil1	pDS111	2b
a	YLS2387	pDS287	pDS220	3b
a	YLS2388	pDS288	pDS220	3b, Supplementary Fig. 3
a	YLS2389	pDS289	pDS220	3b
a	YLS2390	pDS290	pDS220	3b
a	YLS2391	pDS287	pDS221	3b
a	YLS2392	pDS288	pDS221	3b
a	YLS2393	pDS289	pDS221	3b
a	YLS2394	pDS290	pDS221	3b
a	YLS2407	pDS287	pDS282	3b
a	YLS2408	pDS288	pDS282	3b
a	YLS2409	pDS289	pDS282	3b
a	YLS2410	pDS290	pDS282	3b
a	YLS2377	pDS271	pDS220	3c,d; Supplementary Table 1
a	YLS2378	pDS272	pDS220	3c,d; Supplementary Table 1
a	YLS2379	pDS271	pDS221	3c,d; Supplementary Table 1,2
a	YLS2380	pDS272	pDS221	2a; 3c,d; Supplementary Table 1,2
c	YLS1180	pDS255	pDS206	4b, Supplementary Figure 8
c	YLS1181	pDS255	pDS244	4b, Supplementary Figure 8
c	YLS1182	pDS257	pDS190	4b, Supplementary Figure 8
c	YLS1183	pDS257	pDS206	4b, Supplementary Figure 8
c	YLS1184	pDS257	pDS244	4b, Supplementary Figure 8
c	YLS1192	pDS275	pDS206	4b, Supplementary Figure 8
c	YLS1193	pDS275	pDS244	4b, Supplementary Figure 8
c	YLS1195	pDS277	pDS206	4b, Supplementary Figure 8
c	YLS1196	pDS277	pDS244	4b, Supplementary Figure 8

d	YLS2445	pDS250	pDS299	4c
d	YLS2446	pDS250	pDS300	4c,d
d	YLS2447	pDS250	pDS301	4c
a	YLS2415	pDS291	pDS220	Supplementary Fig. 5
a	YLS2416	pDS292	pDS220	Supplementary Fig. 5
a	YLS2417	pDS293	pDS220	Supplementary Fig. 5
a	YLS2418	pDS294	pDS220	Supplementary Fig. 5
a	YLS2419	pDS291	pDS221	Supplementary Fig. 5
a	YLS2420	pDS292	pDS221	Supplementary Fig. 5
a	YLS2421	pDS293	pDS221	Supplementary Fig. 5
a	YLS2422	pDS294	pDS221	Supplementary Fig. 5
e	YLS1128	pDS240	pDS191	Supplementary Fig. 6
e	YLS1131	pDS240	pELW1040	Supplementary Fig. 6
e	YLS2312	pDS240	pDS196	Supplementary Fig. 6
e	YLS2314	pDS240	pDS197	Supplementary Fig. 6
e	YLS2316	pDS240	pDS177	Supplementary Fig. 6
e	YLS2318	pDS240	pDS206	Supplementary Fig. 6
e	YLS2322	pDS240	pDS190	Supplementary Fig. 6
e	YLS2337	pDS250	pDS190	Supplementary Fig. 7a
e	YLS2388	pDS247	pDS206	Supplementary Fig. 7a
e	YLS2389	pDS248	pDS206	Supplementary Fig. 7a
e	YLS2390	pDS250	pDS206	Supplementary Fig. 7a
e	YLS2391	pDS247	pDS244	Supplementary Fig. 7a
e	YLS2392	pDS248	pDS244	Supplementary Fig. 7a
e	YLS2393	pDS250	pDS244	Supplementary Fig. 7a
f	YLS1220	pDS250	pELW1040	Supplementary Fig. 7b
f	YLS1221	pDS250	pDS191	Supplementary Fig. 7b

background strains

a JK9–3d (*MAT***a**/α *leu2–3,112 ura3–52 rme1 trp1 his4*)

b BY4741 (*MAT***a** *his3Δ1 leu2Δ0 met15Δ0 ura3Δ0*)

c YLS2067 (JK9–3d *MAT***a** P_{FUS1}–DsRedMax::*TRP1*)

d YLS1254 (W303 *MAT***a** *trp1*Δ::Gal4-rMR Abp1-mCherry::*HIS3MX*)

e JK9–3d (*MAT***a** *leu2–3,112 ura3–52 rme1 trp1 his4*)

f W303 (*MAT***a** *leu2–3,112 trp1–1 can1–100 ura3–1 ade2–1 his3–11,15*)

Supplementary Table 5 Suggested primers for TULIPs plasmids

Primer	Sequence (5' – 3')	Used for insertion at
F1 (forward)	gat atc aag ctt atc gat acc gtc gac ATG xxx xxx xxx xxx xxx	SalI (all plasmids)
R1 (reverse)	tc tcc ttt act cat tgt cga ggt cga cgc xxx xxx xxx xxx xxx	SalI (before GFP–LOVpep)
R2 (reverse)	cc aag ttc tgg cat tgt cga ggt cga cgc xxx xxx xxx xxx xxx	SalI (before PDZ or ePDZ)
F2 (forward)	att aac tac cgt acc tct aga ctc gag xxx xxx xxx xxx xxx	XhoI (after ePDZ)
F3 (forward)	agg gtt gaa aaa gac tct aga ctc gag xxx xxx xxx xxx xxx	XhoI (after PDZ)
R3 (reverse)	gtg aca taa cta att aca tga ctc gag xxx xxx xxx xxx xxx	XhoI (after PDZ or ePDZ)

Notes:

1. The suggested primers have sufficiently long tails for recombination cloning in yeast. In our experience, these tails also work for InFusion cloning, but shorter (15 bp) tails may improve efficiency. Consult the InFusion protocol (Clontech) for more details.
2. Nucleotide triplets in the primer sequences are in frame with codon triplets in the expected open reading frame of the fusion protein. Required start codons are in capitals.
3. xxx xxx … represents the specific sequence for the inserted gene.
4. The restriction site used for cloning is underlined. The site can usually be killed by mutating the 3’ nucleotide in the primer.

Supplementary Note 1

Peptide epitope design considerations

The Erbin PDZ domain binds specifically to the last four amino acids of a peptide (–3 to 0). In ePDZ fusions the specificity is extended to include the last eight amino acids (–7 to 0), but most of the binding energy derives from specific interactions with the last five amino acids[1]. Notably, the sequence specificity of ePDZ is somewhat relaxed in the –4 to –7 positions, and we reasoned that these amino acids should be selected to be compatible with both Jα docking and ePDZ binding.

One important limitation of the current implementation is that ePDZ proteins only bind to C-terminal peptides; thus, LOVpep must be used as a C-terminal tag. However, ePDZ is functional as either an N- or C-terminal tag. A second potential limitation is that ePDZ or the peptide epitope may interact with endogenous PDZ domains or targets[2]. However, we have not detected such interactions in HeLa cells (**Supplementary Fig. 5**).

Construction of register series

We designed a series of five AsLOV2–peptide fusions for initial screening (**Supplementary Fig. 2a**). Because increased Jα docking affinity improves switching in designed AsLOV2-based photoswitches, we used an AsLOV2 variant with two helix stabilizing mutations, G528A and N538E, as a starting point for our fusions[3]. We used a seven amino-acid peptide epitope (SSADTWV–COOH) that retains the last four amino acids of the high affinity sequence (GSIDTWV–COOH)[1] but has more "neutral" amino acids in the –6 to –4 positions. In particular, we were concerned that the glycine at –6 would disrupt helix formation in the docked state, thereby uncaging the peptide. We therefore substituted a serine at this position, which selection experiments have shown to also have high-affinity binding[1]. We were also concerned that the bulky isoleucine at –4 would interfere with helix docking in shorter constructs. We substituted an alanine at this position, which is known to substantially reduce affinity. However, we felt that this concern was outweighed by the benefit of avoiding potential uncaging. We appended the peptide epitope (–SSADTWV–COOH) to serial truncations of the Jα helix. In the longest of these fusions (Register 1), one amino acid overlaps the end of the Jα helix. We did not explore AsLOV2–peptide fusions shorter than Register 5 because mutation of Ile539 constitutively undocks the Jα helix[4].

For the longest AsLOV2–peptide fusions (Registers 1–3), $\langle R_{obs} \rangle$ was relatively high in both the dark and photoexcited states, and photoswitching was slight (**Supplementary Fig. 2b**). The notable exception was the case of Register 1 paired with ePDZb1. Binding was diminished for the shorter fusions (Registers 4 & 5), probably because more of the epitope is masked in the Jα-docked conformation. Both constructs exhibited greater binding in the lit state than in the dark, indicating light-directed plasma membrane recruitment of ePDZ–mCherry. Register 5 showed less binding than Register 4, suggesting that masking larger regions of the epitope leads to greater caging. It is unclear

why the Register1–ePDZb1 construct undergoes photoswitching; potentially it is because adventitious interactions between ePDZb1 and Jα-derived residues increase the effective size of the epitope beyond eight residues.

Sequence of LOVpep

Once settling on the Register 4 construct, we modified it so as to make the sequence more favorable for ePDZ binding and LOV–Jα docking (LOVpep, **Supplementary Fig. 2a**). In particular, at position –4 valine is strongly favored over alanine for ePDZ binding[1]. Because the corresponding position in the LOV domain (543) is conserved as either valine or alanine, we reasoned that this mutation would not affect helix docking very much. Conversely, ePDZ binding shows little discrimination at position –5 and –6[1]. We therefore mutated the serine at –5 to alanine because alanine is conserved at this position (542) in LOV2 domains, and we mutated the serine at –6 to lysine to introduce a potentially helix-stabilizing *i*, *i* – 4 salt bridge with the glutamate at LOV2 position 537[3]. Specifically, "LOVpep" comprises residues 404–540 of AsLOV2, including the G528A and N538E mutations, fused to the C-terminal peptide KAVDTWV–COOH.

Mutational tuning of affinity

We asked whether mutations in the peptide epitope that weaken binding of model peptides *in vitro* (V–4A and T–2S[1]) would also show lower $<R_{obs}>$ in our *in vivo* assay (**Supplementary Fig. 6**). As in the register series assay, we used ePDZb1–mCherry and ePDZb–mCherry as the recruited proteins. Although the mutations behave somewhat differently in ePDZb and ePDZb1, the V–4A and T–2S mutations usually showed diminished binding; the V–4A,T–2S double mutant showed less than either single mutation. For any given peptide mutation, ePDZb1 usually showed higher binding than ePDZb. In *in vitro* assays, ePDZb1 binds to model peptides an average of 10-fold more tightly than ePDZb, and the V–4A mutation diminishes binding by 110-fold on average[1]. Although we clearly detect the expected trends in binding affinity, the magnitude of the change in $<R_{obs}>$ is comparatively small. This difference may reflect an inherent insensitivity in our assay, or it may indicate that ePDZ interacts with LOVpep differently than with model peptides.

Supplementary Note 2

Suggested workflow for using the TULIPs system

Because tagging can interfere with function for unexpected and unknown reasons, we suggest using the TULIPs system in an initially exploratory way based on few assumptions. We favor tagging multiple potential targets in parallel, in case the tagging inactivates the first choice target. We suggest testing whether GFP–LOVpep tags are functional and accessible for binding by testing recruitment of ePDZ–mCherry constructs. We also suggest testing the effects of recruitment using a constitutively active LOVpep allele expressed from an inducible promoter. This strategy makes it unnecessary to do light-dark experiments initially, and can demonstrate whether a particular configuration is capable of activating a pathway by recruitment.

Once particular tagging strategies have been proven functional, we suggest screening a range of affinity and caging mutations for the best activity. It is important to realize that background binding in the dark state may not be eliminated. We therefore suggest using inducible or repressible promoters whenever there is a possibility that the effects of recruitment will be selected against during strain propagation. Expression levels can affect the degree of binding in both light and dark. If no light dependent effect is observed, try increasing the level of expression. Conversely, if dark activation is too great, try reducing the expression level. We have found that high expression of plasma membrane-bound LOVpep and low expression of cytoplasmic ePDZ–mCherry generally works well for achieving strong recruitment. However, we note that the Mid2(SS/TM)–GFP–LOVpep constructs used in our signal transduction experiments (**Fig. 3**) recruit ePDZ–mCherry very weakly (data not shown) compared to the full-length Mid2–GFP–LOV constructs used in the visual recruitment assays (*e.g.*, **Fig. 2b**).

References for Supplementary Notes

1. Huang, J., Makabe, K., Biancalana, M., Koide, A. & Koide, S. Structural basis for exquisite specificity of affinity clamps, synthetic binding proteins generated through directed domain-interface evolution. *J. Mol. Biol.* **392**, 1221–1231 (2009).
2. Huang, J., Koide, A., Makabe, K. & Koide, S. Design of protein function leaps by directed domain interface evolution. *Proc. Natl. Acad. Sci. USA* **105**, 6578–6583 (2008).
3. Strickland, D. *et al*. Rationally improving LOV domain-based photoswitches. *Nat. Methods* **7**, 623–626 (2010).
4. Harper, S.M., Christie, J.M. & Gardner, K.H. Disruption of the LOV-Jalpha helix interaction activates phototropin kinase activity. *Biochemistry* **43**, 16184–16192 (2004).